Chapter 4

Extending the OptiMorph model in 2D

In the last chapter, we have found a strategy to couple our morphodynamic model with any wave model capable of producing time/spectral averaged wave quantities. We integrated wave calculations from SWAN, XBeach and Shallow-Water into our model, and compared the morphodynamic results with 1D hydro-morphodynamic references from LIP and SANDS, as well as with open-ocean simulations. In this chapter, we develop the 2D model in a straightforward manner. We then carry out morphodynamic simulations reproducing the COPTER 2D basin experiment. Finally, we discuss the sensitivity of the wave model to our morphodynamic results.

Current chapter contents

1 Introduction

The extension of our morphodynamic model to a higher dimension opens up a much wider range of applications: from simple simulations on a 1D real seabed to simulations on 2D more complex seabeds with structures that attenuate wave effects.

Unlike 1D, 2D takes into account a wider range of wave effects. Aspects such as diffraction, refraction and swell angle must not be neglected. It is therefore important to couple our morphodynamic model with a powerful hydrodynamic model that can handle 2D effects. Many 2D models handle these 2D effects and are capable of generating averaged water levels (D. J. Roelvink et al. 2010; Booij et al. 1996; James Thornton Kirby et al. 1994). In this chapter, simulations will mainly be carried out using the REF/DIF: refraction/diffraction model (James Thornton Kirby et al. 1994). However, the user is free to use the morphodynamic model with the hydrodynamic model he prefers.

In numerical models, the transition from a 1D to a 2D model is often a tricky step. In fact, it is often necessary to develop the theory anew and redo the code from scratch. For example, in finite volumes, it is necessary to rewrite the equation model and all the numerical schemes, then implement them. In our case, this step has the advantage of being relatively easy. Indeed, the morphodynamic equation (4.2) has the advantage of being global and therefore always functional in 2D without change.

In this chapter, we will first see how the model has been extended to dimension 2 and its validity in 2D. Then, we will then carry out simulations on the Copter basin configuration in 2D. Finally, we discuss the sensitivity of the wave model to our morphodynamic results.

2 Upgrade OptiMorph Model to 2D

The OptiMorph 2D model will operate in a similar way to the 1D model. It will retain all its versatility, always being able to be coupled with any 2D hydrodynamic model. In this thesis, calculations will be performed on simple square grids, although implementation on triangular grids may be possible in the future. However, this is not the aim of the thesis.

2.1 2D Wave Model

In the previous chapter 3, we demonstrated that the calculation of the gradient $\nabla_\psi \mathcal{J}$ was possible in 1D using the Hadamard approach. The transition to 2D is described in section 2.3. As a result, any 2D hydrodynamic model can be implemented in our code. The choice of hydrodynamic model is decisive in obtaining interesting morphodynamic results. 2D effects such as diffraction and reflection must therefore be taken into account.

The REF/DIF models (James Thornton Kirby et al. 1994) is very well suited to this type of phenomenon. This model is coupled between a refraction part and a diffraction part. It solves the mild-slope equation of Berkhoff (1972) and a dissipation equation. It should be noted that this model provides accurate results for the wave field on bed slopes ranging from 0 to about 1/3. More details on hydrodynamic models are provided in chapter 2, section 4.4, including a detailed presentation of the REF/DIF models.

2.2 2D Morphodynamic Model

The advantage of a global morphodynamic model makes it usable in any space without any changes. We recall below the definition of the functional $\mathcal{J}$ (J s m^{-1}). For all $t \in [0, T_f]$, we have:

$$\mathcal{J}(\psi, t) = \frac{1}{16} \int_{t-T_{coupl}}^{t} \int_{\Omega} \rho_w g H^2(\psi, x, y, \tau) \mathrm{d}x\mathrm{d}\tau, \tag{4.1}$$

where H denotes the height of the waves over the 2D domain Ω (m^2), ρ_w is water density (kg m^{-3}), and g is the gravitational acceleration (m s^{-2}). T_{coupl} (s) defines the coupling time interval between hydrodynamic and morphodynamic models so that we have T_f / T_{coupl} iterations.

As explained above, the morphodynamic equation (4.2) remains the same,

$$\begin{cases} \psi_t = \Upsilon \, \Lambda \, d \\ \psi(t=0) = \psi_0. \end{cases} \tag{4.2}$$

The initial state ψ_0 is defined on $\mathbb{R}^2$, ψ_t is the evolution of the bottom elevation over time (m s^{-1}) (also defined on $\mathbb{R}^2$), Υ is a measure of the sand mobility expressed in m s kg^{-1} (also defined on $\mathbb{R}^2$), Λ measures the excitation of the seabed by the orbital motion of water waves, and d is the direction of the descent (J s m^{-2}), which indicates the manner in which the sea bottom changes. In unconstrained configurations, there would be $d = -\nabla_\psi \mathcal{J}$, which by its definition indicates the direction of a local minimum of $\mathcal{J}$ with respect to ψ as illustrated in figure 1.5 in 1D.

2.3 2D Hadamard Derivative

In this section, we explain the calculation of the gradient with respect to the shape ∇_ψ, in 2D, in a similar way to the previous chapter 3. On the one hand, we will look at the mathematical developments. On the other, we will look at the 2D numerical validation, and thus at the limits of this strategy.

2.3.1 Mathematical Background

The Hadamard strategy introduced in the previous chapter 3 has been written in multi-dimensional (section 3). Using the equation (5.21) with $\nabla_X \mathcal{J} = \left(\frac{\partial \mathcal{J}}{\partial x}, \frac{\partial \mathcal{J}}{\partial y}, \frac{\partial \mathcal{J}}{\partial \psi}\right)^\intercal$ we obtain the new equation:

$$\nabla_\psi \mathcal{J} \approx \frac{\partial \mathcal{J}}{\partial x} n_x + \frac{\partial \mathcal{J}}{\partial y} n_y + \frac{\partial \mathcal{J}}{\partial \psi} n_z \tag{4.3}$$

with n_x, n_y and n_z the x, y and z component of n. The vector n is calculated on each component i, j of the grid as the vector product of two non-collinear vectors of the plane generated by the 3 points associated to $(\psi_{i+1,j}, \psi_{i,j}, \psi_{i,j+1})$ (see figure 4.3).

2.3.2 Numerical Validation

1D numerical validation was carried out in the previous chapter 3 section 3.3. The 2D extension does not change the validity of our Hadamard strategy. Two simple 2D validation cases are shown in figures 4.1 and 4.2. In these cases, we use the simple shoaling model presented in equations (1.2a). This allows us to directly compare the analytical solution $\nabla_\psi H$ with the numerical one. In the first case, we assume a linear seabed. In the second 4.2, we add a bump to induce non-linearity.

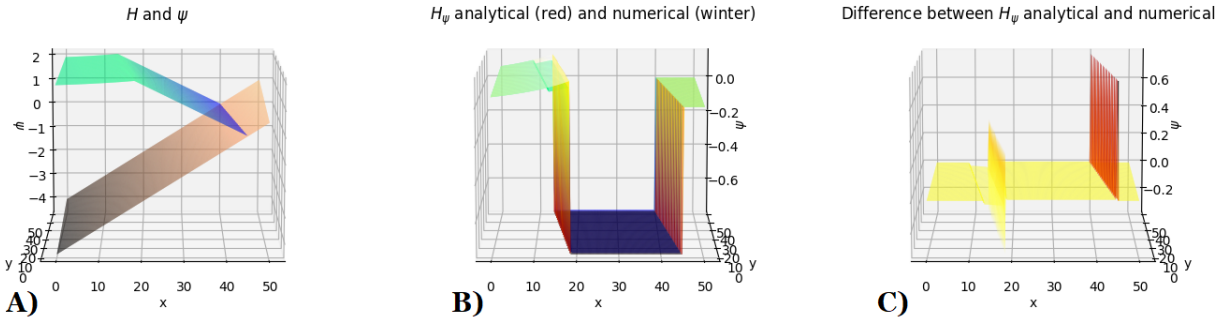

Figure 4.1 – OptiMorph 2D using Hadamard with multi-1D simple shoaling models with linear bottom elevation. A) Seabed and Wave Height B) Superposition of analytical and numerical gradients C) Differences between analytical and numerical gradients.

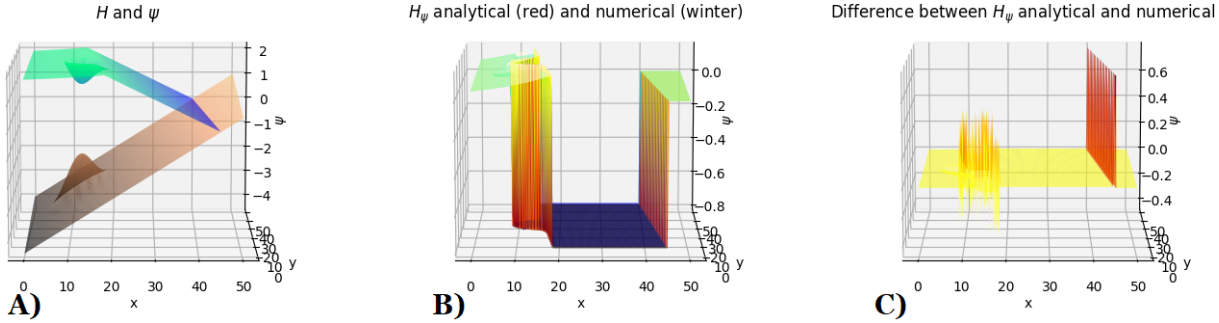

Figure 4.2 – OptiMorph 2D using Hadamard with multi-1D simple shoaling models with linear bottom elevation + geotube. A) Seabed and Wave Height B) Superposition of analytical and numerical gradients C) Differences between analytical and numerical gradients.

The results 4.1.C and 4.2.C show that the model is very robust over the whole Ω domain. However, some difficulties are encountered on the non-linear parts of ψ and H. This can be explained by the fact that the n normal vectors are often miscalculated in these parts.

2.4 2D Constraints

The two constraints of the model are easily transformed into 2D. The first is the slope constraint, which ensures that there are no unrealistic slopes in the model. The second is the sand conservation constraint, which is useful in experimental configurations, for example.

2.4.1 Slope Constraint

The 2D slope constraint becomes slightly more complex than in 1D (equation (5.23)). In fact, it is necessary to take into account the maximum slope according to $\vec{x}$ (red nodes on figure 4.3),

$$\left|\frac{\partial \psi}{\partial x}\right| \leq M_{\text{slope}}, \tag{4.4}$$

according to $\vec{y}$ (blue nodes on figure 4.3),

$$\left|\frac{\partial \psi}{\partial y}\right| \leq M_{\text{slope}}, \tag{4.5}$$

and also on the diagonals along $\vec{a}$ and $\vec{b}$ (green nodes on figure 4.3),

$$\left|\frac{\partial \psi}{\partial a}\right| \leq M_{\text{slope}}, \quad \text{and} \quad \left|\frac{\partial \psi}{\partial b}\right| \leq M_{\text{slope}}. \tag{4.6}$$

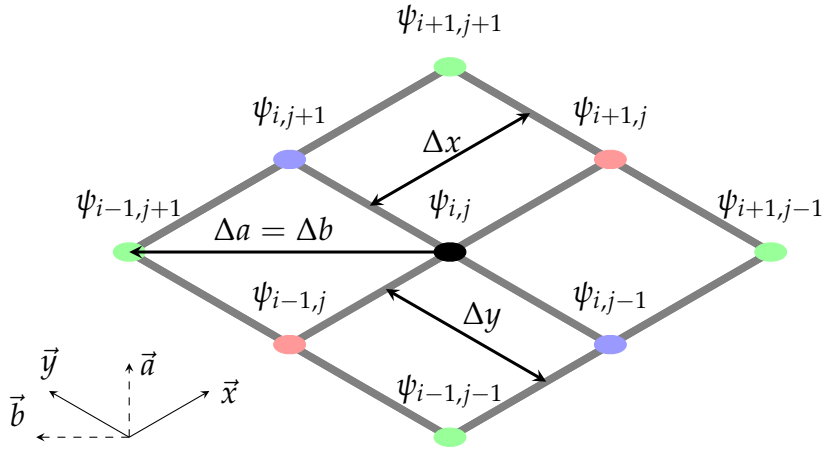

Figure 4.3 – Nodes representation.

2.4.2 Sand Conservation Constraint

The sand conservation constraint remains the same. The integration of the Ω domain simply switches from 1D to 2D as illustrated in the following equation (4.7).

$$\int_{\Omega} \psi(t,x,y)\mathrm{d}\Omega = \int_{\Omega} \psi_0(x,y)\mathrm{d}\Omega, \qquad \forall t \in [0, T_f], \tag{4.7}$$

with ψ the seabed at time t and ψ_0 the initial seabed.

3 2D Applications

Contrary to the previous chapter, 2D morphodynamic data are very rare. Most 2D validations are carried out in 1D: LIP, SANDS, Duck, etc. It is therefore difficult to obtain 2D morphodynamic validation data, so we will use 2D Copter data (Bouchette 2017), whose 1D data were used in the chapter 1. We will then carry out an application with a linear seabed by adding a geotextile tube as was done in the multi-1D section 4 of the chapter 1.

3.1 Presentation of the Copter 2D experience

The 2D Copter experiment (Bouchette 2017) has been conducted in the 30 m x 30m LHF wave basin in Grenoble (see Figure 4.4A) with a length scale of 1/10 and a time scale 1/3 (obtained with Froude scaling).
The sediment parameters that have been used in the present experiments are as follows: the density of 2 650 kg/m^3 and median diameter d_{50} = 0.166 mm. This choice leads to

fulfill a Rouse scaling for a prototype grain size of $d_{50}\approx$0.3 mm.

The beach morphology was measured by means of a laser profiler mounted on a motorized trolley located on a sliding rail 4.4A). This measurement technique required emptying the basin before recording the bed elevation. The seabed elevation was recorded with millimeter accuracy every 10 cm and 1 cm in the alongshore and cross-shore direction, respectively. As shown in the Figure 4.4A)) the bathymetric survey zone was restricted by the sliding rail configuration and covered the area 7.84 m$< x <$ 22.84 m in the cross-shore direction, 3.12 m$< y <$ 28.02 m alongshore.
The free surface elevations were measured by means of 18 capacitance gages.

JONSWAP irregular waves were generated over 20mn sequences, repeated several times. Four typical wave climates are considered:

1. Storm rising: $H_s = 0.17$ m / $T_0 = 2.1$ s,
2. Storm apex: $H_s = 0.23$ m / $T_0 = 2.3$ s,
3. Storm waning: $H_s = 0.18$ m / $T_0 = 3.5$ s,
4. Calm wave conditions: $H_s = 0.11$ m / $T_0 = 2$ s.

In part 2 (Storm apex), a geotube was added as shown in figure 4.4.

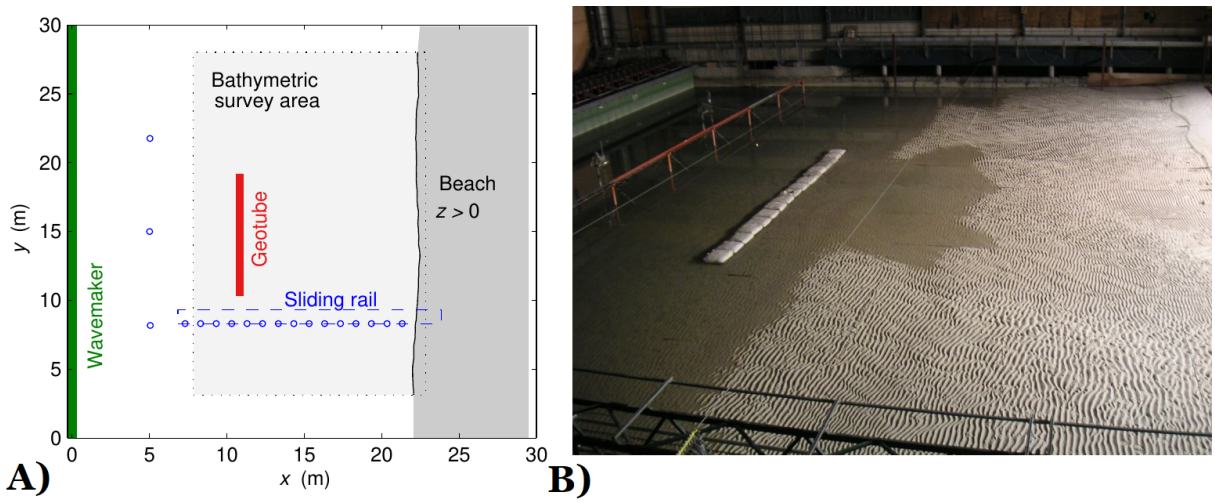

Figure 4.4 – **A)** Schema of Copter's 2D configuration. **B)** Photo of the 2D Copter experiment.

3.2 Application on Copter 2D

To begin, we perform hydro-morphodynamic simulations with our morphodynamic approach using Hadamard's calculation of $\nabla_\psi \mathcal{J}$. To highlight the phenomenological aspect of our model, we start by performing simulations on Copter 2D seabed.

In this case, we set up the models as follows. We set a domain $\Omega = 24.9$ x 15 m with a uniform subdivision in $\vec{x}$ of 50 cells and uniform subdivision in $\vec{y}$ of 50 cells. For REF/DIF and Shoaling multi-1D models, the incoming wave boundary condition is $H_s = 0.23$ m, a wave period $T_0 = 2.3$ s and a wave angle of incidence of 0 degrees, but this can be changed in REF/DIF. The breaker model of the extended Shoaling model is simply based on a W. Munk (1949) breaking criterion $\gamma = 0.78$. The mobility parameter Υ of our morphodynamic model has a value of 4×10^{-2} m.s.kg^{-1}. The model is set to run 20 mins using a coupling time of 24 s. We compare in figure 4.5 the results obtained using the two wave models multi-1D shoaling, REF/DIF and the experimental result.

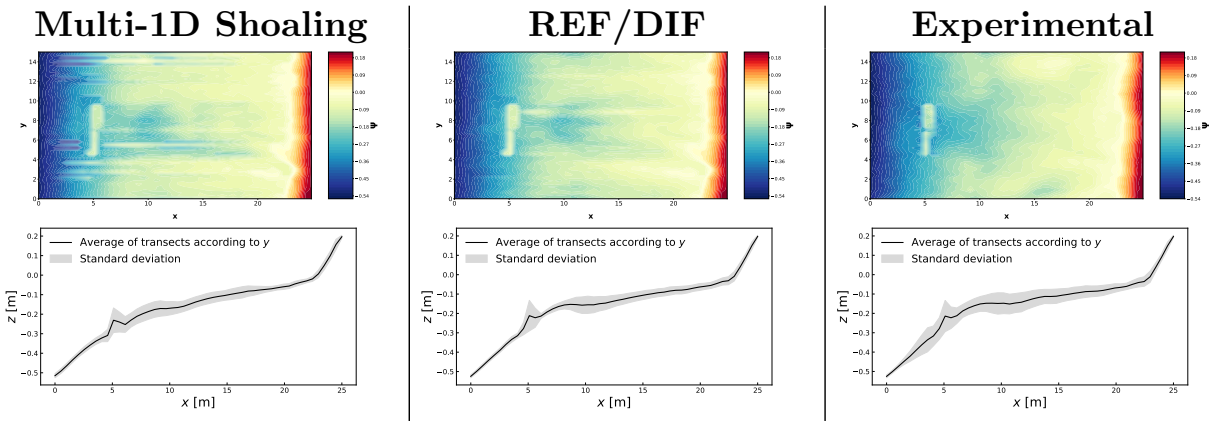

Figure 4.5 – **(Top)** Morphodynamic results using OptiMorph in 2D using the Multi-1D Shoaling model (left), REF/DIF (center) and comparing with experiments (right). **(Bottom)** Variability of the transects (in $\vec{x}$ direction) with the mean (black) and standard deviation (gray).

In all three figures, a trough is visible at the rear of the geotube. The variability of morphodynamic results with the multi-1D Shoaling model and the experiment is much greater than that of REF/DIF.

3.3 Linear Seabed with Geotube

In this case, we set up the models as follows. We set a domain Ω =600 x 20 m with a uniform subdivision in $\vec{x}$ of 300 cells and uniform subdivision in $\vec{y}$ of 60 cells. For REF/DIF and Shoaling multi-1D models, the incoming wave boundary condition is $H_0 = 2$ m, a wave period $T_0 = 6$ s and a wave angle of incidence of 0 degrees. The breaker model is the same as in the previous section. The mobility parameter Υ of our

morphodynamic model has a value of 4×10^{-2} m.s.kg^{-1}. The model is set to run 3 day using a coupling time of 5184 s.

The initial seabed is linear (see Figure 4.6), with a $\vec{x}$ slope of 1/100, with the addition of a geotextile tube at $x = 150$ m and a height of 2.5 m.

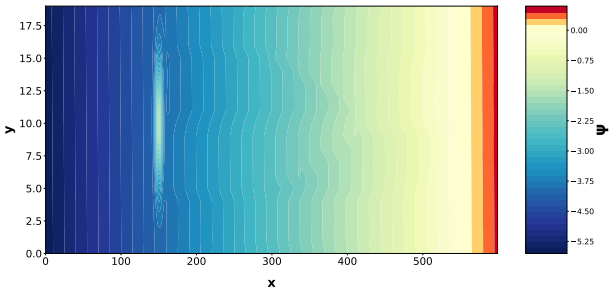

Figure 4.6 – Initial seabed with a linear slope of 1/100 with a geotextile tube at $x = 150$ m.

We compare in figure 4.7 the results obtained using the two hydrodynamic models shoaling / REF/DIF.

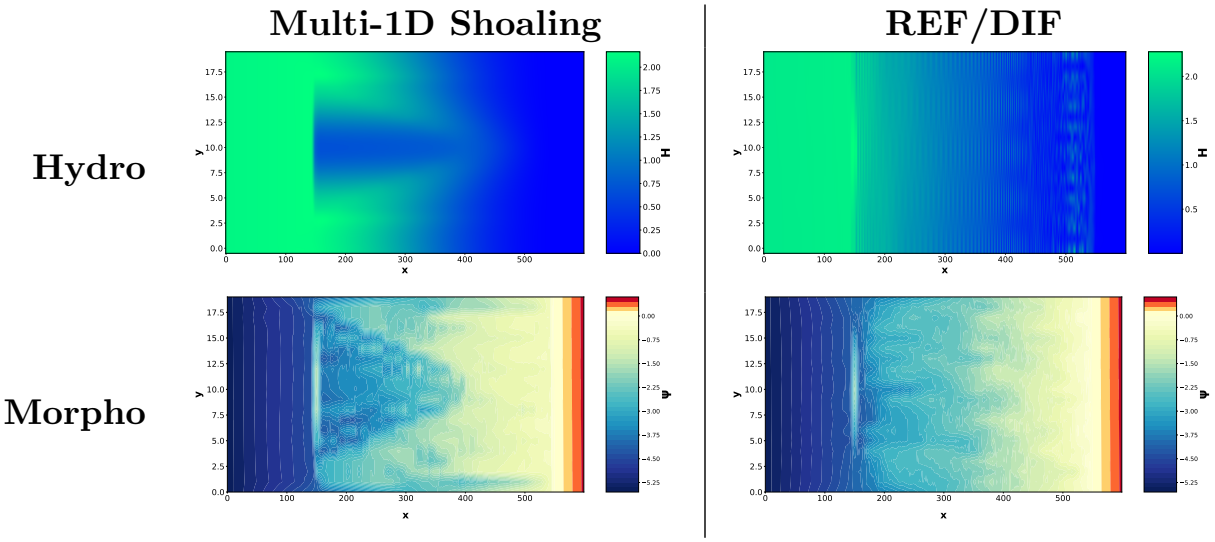

Figure 4.7 – 2D simulation of OptiMorph using Shoaling and REF/DIF models. Linear seabed (1/100) with geotube. Offshore height $H_0 = 2$ m and wave period $T_0 = 6$ s.

Here, the hydro-morphodynamic results produced by the two models are completely different. However, a trough can still be seen behind the geotube. This is much more pronounced using the multi-1D Shoaling model than using the REF/DIF models. Small oscillations are observed on the REF/DIF wave model.

4 Discussion

In Copter's 2D configuration (Bouchette 2017), the geotextile tube can be seen as a sedimentary bar. This leads to the wave breaking prematurely, creating a trough behind the geotube. The morphodynamic model coupled with multi-1D shoaling or REF/DIF reproduces this behaviour with the break in the slope behind the structure, as shown in figure 4.5. This result can also be seen in figure 4.7 and it was also illustrated in the chapter 1 in the section 4, as well as in the results in the chapter 3. For morphodynamic results with the multi-1D shoaling models (figure 4.5 left), non-linearities are observed between transects. This is due to the variability between transects (figure 4.5 left/bottom), as the multi-1D shoaling model calculates the hydrodynamics on each transect without taking 2D effects into account.

To obtain consistent morphodynamic results, it is very important to choose the associated hydrodynamic model carefully. It must be chosen according to the field of study (type of beach, type of experiment, type of waves, etc.) with the help of specialists. Indeed, the results of figure 4.7 show that two completely different wave models (multi-1D shoaling and REF/DIF), produce completely different morphodynamics. For example, the breaking of the REF/DIF wave model is very steep and therefore induces localised sediment transport below this wave breaking (justification in the section 5.4). This is in contrast to the multi-1D model, which has a smoother breaking, resulting in greater sediment movement behind the geotube. This strategy is in line with Murray (2007) who explains that there is no universal morphodynamic model, and that it is necessary to choose carefully on a case-by-case basis.

5 Conclusion

In this chapter, we looked at the implementation of the OptiMorph 2D model. Due to the global scale of this model, implementation is very straightforward. The 2D model is validated in a similar way to the 1D model. An application on the Copter 2D configuration (Bouchette 2017) has been performed. In this case, the geotextile tube acts like a sedimentary bar and as a result, a trough is formed behind this geotube. The model has been able to reproduce this behaviour qualitatively. Dealing with complex problems, this model can therefore be used in coastal engineering involving wave dissipation structures. However, the choice of the wave model must be made with greater knowledge of the study case to avoid obtaining inconsistent morphodynamic results. In the future, it will be very important for users to choose the 2D wave model carefully.

Chapter key points

- Straightforward implementation of the 2D model.
- Several applications using multi-1D Shoaling and REF/DIF wave models.
- A model capable of managing complex structures on the seabed.
- Morphodynamic sensitivity due to wave models.